J|A|C|S ARTICLES

Published on Web 10/26/2010

Theoretical Study on the Repair Mechanism of the (6−4) Photolesion by the (6−4) Photolyase

Keyarash Sadeghian,[†] Marco Bocola,[‡] Thomas Merz,[†] and Martin Schütz*,[†]

Institute of Physical and Theoretical Chemistry and Institute of Biophysics and Physical Biochemistry, University of Regensburg, Universitätsstraβe 31, D-93040 Regensburg, Germany

Received September 15, 2010; E-mail: martin.schuetz@chemie.uni-regensburg.de

Abstract: UV irradiation of DNA can lead to the formation of mutagenic (6−4) pyrimidine−pyrimidone photolesions. The (6−4) photolyases are the enzymes responsible for the photoinduced repair of such lesions. On the basis of the recently published crystal structure of the (6−4) photolyase bound to DNA [Maul et al. 2008] and employing quantum mechanics/molecular mechanics techniques, a repair mechanism is proposed, which involves two photoexcitations. The flavin chromophore, initially being in its reduced anionic form, is photoexcited and donates an electron to the (6−4) form of the photolesion. The photolesion is then protonated by the neighboring histidine residue and forms a radical intermediate. The latter undergoes a series of energy stabilizing hydrogen-bonding rearrangements before the electron back transfer to the flavin semiquinone. The resulting structure corresponds to the oxetane intermediate, long thought to be formed upon DNA−enzyme binding. A second photoexcitation of the flavin promotes another electron transfer to the oxetane. Proton donation from the same histidine residue allows for the splitting of the four-membered ring, hence opening an efficient pathway to the final repaired form. The repair of the lesion by a single photoexcitation was shown not to be feasible.

1. Introduction

Solar irradiation in the UV spectral range (290−320 nm) is responsible for the formation of mutagenic photolesions from adjacent pyrimidine bases in DNA,[1,2] which may then lead to harmful and even lethal effects such as growth delay and skin cancer.[3−5] There are two major types of photoproducts, *cis*−*syn* cyclobutane pyrimidine dimer (CPD) and (6−4) pyrimidine−pyrimidone (6−4) (Figure 1), both formed as a result of covalent bond formation between neighboring pyrimidine bases.[6]

Nature has developed light-dependent enzymes, known as CPD- and (6−4) photolyase, which are able to recognize DNA double-strands containing photolesions and to repair them.[7−10] Photolyase enzymes utilize efficient light-harvesting antenna chromophores such as methenyltetrahydrofolate (MTHF) or 8-hydroxy-7,8-didemethyl-5-deazariboflavin (8-HDF) and are thereafter classified as either a folate- or a deazaflavin-photolyase.[11] The flavin adenine dinucleotide (FAD) chromophore, also found in photolyase enzymes, is a vital component for the repair process and is usually found in its anionic reduced form $FADH^-$. The initial steps in the photolyase-mediated repair consist of blue-light absorption by the antenna (MTHF/8-HDF), energy transfer from the latter to the $FADH^-$, followed by electron transfer from $FADH^-$ to the photolesion.[12] This is the common feature among both CPD and (6−4) photolyase enzymes. The repair pathways for CPD and (6−4) photoproducts, however, go in separate directions after the electron injection from $FADH^-$. In the CPD case, the two covalent C5−C5′ and C6−C6′ bonds (see Figure 1 for numbering) need to be cleaved. The whole repair process, that is, forward electron transfer, ring splitting, and backward electron

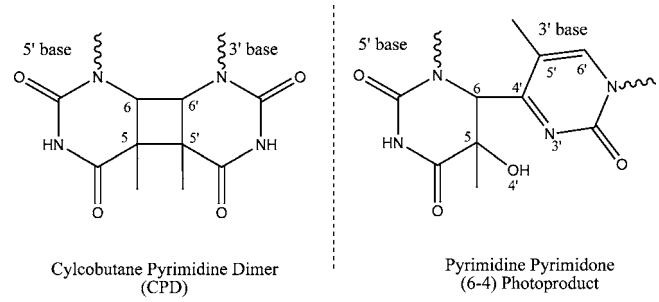

Figure 1. Left: *cis*,*syn*-cyclobutane pyrimidine dimer, CPD (here thymine). Right: (6−4)T−T photoproducts.

[†] Institute of Physical and Theoretical Chemistry.
[‡] Institute of Biophysics and Physical Biochemistry.

(1) Mitchell, D. L.; Nairn, R. S. *Photochem. Photobiol.* **1989**, *49*, 805–809.
(2) Taylor, J. S. *Acc. Chem. Res.* **1994**, *27*, 76–82.
(3) Vink, A. A.; Roza, L. *J. Photochem. Photobiol., B* **2001**, *65*, 101–104.
(4) Pouget, J. P.; Douki, T.; Richard, M. J.; Cadet, J. *Chem. Res. Toxicol.* **2000**, *13*, 541–549.
(5) Brash, D. E.; Rudolph, J. A.; Simon, J. A.; Lin, A.; McKenna, G. J.; Baden, H. P.; Halperin, A. J.; Ponten, J. *Proc. Natl. Acad. Sci. U.S.A.* **1991**, *88*, 10124–8.
(6) Sinha, R. P.; Hader, D. P. *Photochem. Photobiol. Sci.* **2002**, *1*, 225–226.
(7) Sancar, A. *Chem. Rev.* **2003**, *103*, 2203–2207.
(8) Weber, S. *Biochim. Biophys. Acta* **2005**, *1707*, 1–23.
(9) Essen, L. O.; Klar, T. *Cell. Mol. Life Sci.* **2006**, *63*, 1266–1267.
(10) Boussicault, F.; Robert, M. *Chem. Rev.* **2008**, *108*, 2622–2625.
(11) Sancar, A.; Sancar, G. B. *Annu. Rev. Biochem.* **1988**, *57*, 29–67.
(12) Kao, Y. T.; Saxena, C.; Wang, L.; Sancar, A.; Zhong, D. *Proc. Natl. Acad. Sci. U.S.A.* **2005**, *102*, 16128–32.

transfer, is completed within a nanosecond.[13] There are numerous studies dealing with the reaction kinetics and barriers involved in the repair of CPD via CPD-photolyase, which include transient spectroscopy measurements,[12,14,15] as well as theoretical calculations, which are all discussed in an excellent review by Harrison et al.[16] One should also mention the recent quantum mechanics/molecular mechanics (QM/MM) studies reported by Masson et al. regarding the repair of CPD photolesion with and without the assistance of the CPD photolyase enzyme.[17,18]

The (6−4)T−T photoproduct, being the main topic of this work, is thought to be formed via a [2 + 2] cycloaddition of the C4 carbonyl of the 3′ thymine base with the 5−6 double bond of the neighboring 5′ thymine base, hence forming the so-called oxetane intermediate. The latter species, being unstable at temperatures above −80 °C, forms the corresponding (6−4) open form after cleavage of the C4′−O4′ bond.[19] In contrast to the relatively "straightforward" repair of the CPD photolesion, which mainly involves a consecutive or concerted rupture of the two C−C bonds, the repair of the (6−4)T−T photolesion is not yet fully understood. Kim et al.[20] suggested a two-step repair mechanism, which consists of (i) a thermally driven step where the four-membered ring oxetane is formed upon binding of the DNA−substrate with the photolyase-enzyme, and (ii), a photochemically driven step involving the ring-opening of the latter intermediate upon electron uptake from the $FADH^-$ chromophore. According to the aforementioned mechanism of the (6−4)T−T formation, the open-form species must be more stable than the four-membered oxetane intermediate. In fact, this has already been shown by the theoretical gas-phase calculations of Heelis et al.[21] Yet Hitomi et al.[22] proposed that the formation of the oxetane/azetidine intermediate may well be catalyzed by the two highly conserved histidine amino acids in the photolesion binding pocket of the (6−4) photolyase upon binding.[22] The strong pH dependency of the repair activity (maximum activity at pH 8.5) has led these authors to the conclusion that both histidines play a crucial role in the thermally driven formation of the four-membered ring intermediate. By substitution at the N3′ position of the 3′-base, Asgatay et al. claim to have found evidence for the (6−4)T−T repair via an oxetane intermediate.[23] Yamamoto et al.,[24] on the other hand, propose an oxetane repair pathway by assigning a key role to the 2′-carbonyl group of the 3′-base. Substitution of the C═O group with an imine still allows for binding of the DNA to the (6−4) photolyase, but no repair activity could be detected.[24]

There have been numerous model studies in agreement with an efficient splitting of the oxetane to two thymine monomers as a result of photoexcitation or reduction by an external electron donor.[25−32] Theoretical calculations published to this date mostly concentrate on the reductive/oxidative splitting of the oxetane intermediate[33−35] and have all shown that such a process is quite efficient. Furthermore, there are various measurements on the (6−4) photolyase enzyme without DNA substrate, including time-resolved electron paramagnetic resonance spectroscopy,[36,37] resonance Raman spectroscopy,[38,39] as well as steady-state absorption and fluorescence spectroscopy.[40] Overall, the idea of oxetane-mediated repair of (6−4)T−T has been rather widespread.

The recently published crystal structure of (6−4) photolyase in complex with a (6−4)T−T containing DNA has brought new insight into the structure of the (6−4)T−T photolesion prior to repair.[41] In this crystal structure, no oxetane species could be identified, and the initial structure of the (6−4)T−T photolesion is kept. In other words, the two above-discussed histidine residues, although being in the neighborhood of the photolesion, are not able to thermally transform the latter into a stable oxetane intermediate. A similar observation is also made for the complex of the T(6−4)C photoproduct with the (6−4) photolyase where the corresponding four-membered ring intermediate, azetidine, could not be observed in the crystal structure.[42]

As a consequence, another mechanism for the repair of the (6−4) photoproduct has been proposed by Maul et al. where a different role is attributed to the two histidine residues.[41] It has been suggested that after the electron uptake from the $FADH^-$ chromophore, a water molecule is formed as a result of hydroxyl group detachment from the 5′-T base and deprotonation of the His365 residue. This water molecule is then able to attack the acylimine moiety and to form a stable radical intermediate. After electron back transfer to $FADH^\bullet$ and deprotonation of the radical, the repair process is over and the pyrimidine bases are separated.

(13) Kao, Y. T.; Saxena, C.; Wang, L.; Sancar, A.; Zhong, D. *Proc. Natl. Acad. Sci. U.S.A.* **2005**, *102*, 16128–32.
(14) Langenbacher, T.; Zhao, X.; Bieser, G.; Heelis, P. F.; Sancar, A.; Michel-Beyerle, M. E. *J. Am. Chem. Soc.* **1997**, *119*, 10532–10536.
(15) MacFarlane, A. W.; Stanley, R. J. *Biochemistry* **2003**, *42*, 8558–8558.
(16) Harrison, C. B.; O'Neil, L. L.; Wiest, O. *J. Phys. Chem. A* **2005**, *109*, 7001–7002.
(17) Masson, F.; Laino, T.; Tavernelli, I.; Rothlisberger, U.; Hutter, J. *J. Am. Chem. Soc.* **2008**, *130*, 3443–3450.
(18) Masson, F.; Laino, T.; Rothlisberger, U.; Hutter, J. *ChemPhysChem* **2009**, *10*, 400–410.
(19) Rahn, R. O.; Hosszu, J. L. *Photochem. Photobiol.* **1969**, *10*, 131–137.
(20) Zhao, X.; Liu, J.; Hsu, D. S.; Zhao, S.; Taylor, J. S.; Sancar, A. *J. Biol. Chem.* **1997**, *272*, 32580–90.
(21) Heelis, P. F.; Liu, S. *J. Am. Chem. Soc.* **1997**, *119*, 2936–2937.
(22) Hitomi, K.; Nakamura, H.; Kim, S. T.; Mizukoshi, T.; Ishikawa, T.; Iwai, S.; Todo, T. *J. Biol. Chem.* **2001**, *276*, 10103–9.
(23) Asgatay, S.; Petermann, C.; Harakat, D.; Guillaume, D.; Taylor, J.-S.; Clivio, P. *J. Am. Chem. Soc.* **2008**, *130*, 12618–9.
(24) Yamamoto, J.; Hitomi, K.; Hayashi, R.; Getzoff, E. D.; Iwai, S. *Biochemistry* **2009**, *48*, 9306–9312.
(25) Cichon, M. K.; Arnold, S.; Carell, T. *Angew. Chem., Int. Ed.* **2002**, *41*, 767–770.
(26) Friedel, M. G.; Cichon, M. K.; Carell, T. *Org. Biomol. Chem.* **2005**, *3*, 1937–1941.
(27) Yamamoto, J.; Tanaka, Y.; Iwai, S. *Org. Biomol. Chem.* **2009**, *7*, 161–166.
(28) Song, Q.-H.; Wang, H.-B.; Tang, W.-J.; Guo, Q.-X.; Yu, S.-Q. *Org. Biomol. Chem.* **2006**, *4*, 291–298.
(29) Stafforst, T.; Diederichsen, U. *Chem. Commun.* **2005**, 3430–3432.
(30) Boussicault, F.; Robert, M. *J. Phys. Chem. B* **2006**, *110*, 21987–93.
(31) Joseph, A.; Prakash, G.; Falvey, D. E. *J. Am. Chem. Soc.* **2000**, *122*, 11219–11225.
(32) Miranda, M. A.; Izquierdo, M. A.; Galindo, F. *Org. Lett.* **2001**, *3*, 1965–1967.
(33) Wang, Y.; Gaspar, P. P.; Taylor, J.-S. *J. Am. Chem. Soc.* **2000**, *122*, 5510–5519.
(34) Borg, O. A.; Eriksson, L. A.; Durbeej, B. *J. Phys. Chem. A* **2007**, *111*, 2351–2351.
(35) Izquierdo, M. A.; Domingo, L. R.; Miranda, M. A. *J. Phys. Chem. A* **2005**, *109*, 2602–2607.
(36) Weber, S.; Kay, C. W. M.; Mogling, H.; Mobius, K.; Hitomi, K.; Todo, T. *Proc. Natl. Acad. Sci. U.S.A.* **2002**, *99*, 1319–1322.
(37) Schleicher, E.; Hitomi, K.; Kay, C. W.; Getzoff, E. D.; Todo, T.; Weber, S. *J. Biol. Chem.* **2007**, *282*, 4738–4747.
(38) Li, J.; Uchida, T.; Ohta, T.; Todo, T.; Kitagawa, T. *J. Phys. Chem. B* **2006**, *110*, 16724–32.
(39) Li, J.; Uchida, T.; Todo, T.; Kitagawa, T. *J. Biol. Chem.* **2006**, *281*, 25551–9.
(40) Usman, A.; Brazard, J.; Martin, M. M.; Plaza, P.; Heijde, M.; Zabulon, G.; Bowler, C. *J. Photochem. Photobiol., B* **2009**, *96*, 38–48.
(41) Maul, M. J.; Barends, T. R. M.; Glas, A. F.; Cryle, M. J.; Domratcheva, T.; Schneider, S.; Schlichting, I.; Carell, T. *Angew. Chem., Int. Ed.* **2008**, *47*, 10076–80.
(42) Glas, A. F.; Schneider, S.; Maul, M. J.; Hennecke, U.; Carell, T. *Chemistry* **2009**, *15*, 10387–96.

In the whole process, the two histidine residues assist the formation of the water molecule and provide a channel for the proton transfer processes, which finally leads to the repair of the (6−4)T−T photolesion.[41]

Another interesting non-oxetane mechanism has been proposed by Domratcheva and Schlichting.[43] On the basis of gas-phase calculations on a (6−4)T−T model system in its radical anionic state, the authors propose a direct OH transfer from the 5′- to the 3′-base as the main reaction coordinate for the repair.[43]

In a recent study by Li et al.,[44] the temporal evolution of the $FADH^{\bullet}$ radical intermediate, formed as a result of $FADH^{-} \rightarrow$ (6−4)T−T electron transfer, is mapped out via femtosecond spectroscopy techniques. The lifetime of the $FADH^{\bullet}$ radical is estimated to be in the order of tens of nanoseconds. This important finding will be discussed further below in the context of the mechanism proposed here.

In this contribution, we report on the results of a (QM/MM) study, which was carried out on the repair of the (6−4)T−T photoproduct via (6−4) photolyase. QM/MM techniques have already been shown to be proper tools for describing biochemical reactions in both ground and excited states (for reviews, see refs 45−48). The main idea is to investigate and understand the catalytic function of those amino acids (in the present context the two histidines) found in the vicinity of the photolesion after binding with the enzyme. The current study is, to our best knowledge, the first QM/MM study presented on the repair mechanism of the (6−4) photolesion by the (6−4) photolyase enzyme. Its intention is to screen a selection of steps that are likely to be involved in the repair process based on their energetic feasibility.

2. Computational Details

The crystal structure of the (6−4) photolyase from *Drosophila melanogaster*, bound to a (6−4)T−T photoproduct containing DNA[41] (PDB code 3CVU), has been used as a starting structure for the Molecular Dynamics (MD) simulation. Terminating nucleic bases of the DNA double strand were removed because their complement bases were not resolved in the crystal structure. All crystal water molecules were kept, and 14 Na^{+} counterions were added. After comparing the protonation state and orientation of the residues in the DNA−photolyase with those suggested by the MolProbity software,[49] nitrogen and oxygen atoms in the glutamine residues 55, 123, 286, and 393 were flipped, and all missing hydrogen atoms were added. To study different protonation states of the two His365 and His369 residues, three different system setups were made: (i) neither of these protonated, (ii) only His365 protonated, and (iii) only His369 protonated. The system was then solvated in a TIP3 water[50] box of the size $80 \times 80 \times 80$ Å^3. The AMBER03 force field[51] was employed for the MM description of the photolyase, DNA, and the counterions. The AMBER-10[52] program package was used for the MD simulations. In addition, the reparameterized α/γ torsional term derived for the DNA backbone (parmbsc0)[53] was applied.

For the initial MD simulations, both the FAD chromophore and the (6−4)T−T lesion must be parameterized. For this purpose, point charges for the $FADH^{-}$ chromophore prior to electron transfer, with a total charge of −3 (−1 for each phosphate group and −1 for the flavin moiety) and (6−4)T−T lesion (neutral), were obtained from the restrained electrostatic potential (RESP) fit[54] on top of a HF gas-phase calculation in the 6-31G* basis set. The remaining force field parameters were taken from those available in the AMBER force field database and from the previous study by Masson et al.[18] These parameters are provided in the Supporting Information.

Starting from the minimized solvated structure and restraining the coordinates of the backbone atoms of both DNA and protein, a 20 ps constant volume MD simulation was carried out where the temperature was increased from 0 to 300 K. The simulation was continued by taking the last configuration and performing unrestrained constant pressure MD for 100 ps to equilibrate the system. Finally, a constant pressure (1 atm) and temperature (300 K) MD (1 ns) was performed to gather the simulation data for the analysis.

The MD simulations have shown that the binding pocket of the photolesion is quite stable. A standard pairwise root-mean-square deviation (rmsd) cluster analysis of the MD snap shots was performed using the Ptraj module implemented in AMBER Tools 1.2.[55] A clustering cutoff of 1 Å for the rmsd of those atoms within the active region of the QM/MM setup (vide infra) leads to a single cluster of structures. Therefore, a representative snapshot from this cluster was chosen for the QM/MM investigations. Choosing a clustering cutoff 0.3 Å leads to five clusters; the chosen snapshot, however, belongs to the cluster with the lowest rmsd from the crystal structure. The same hydrogen-bonding network within the photolesion binding pocket is observed across all these clusters. The chosen snapshot can therefore be considered as adequately representative for the subsequent calculations. According to previous studies,[56] the so neglected protein fluctuations may influence the barriers by about 2 kcal/mol. However, as is shown further below, the overall picture of the reaction mechanism is not influenced by deviations of that size.

For the QM/MM calculations, the size of the system was reduced by removing all water molecules that were more than 12 Å away from the reaction center (i.e., the (6−4)T−T photoproduct) as well those water molecules that are more than 5 Å away from the protein and DNA. The counterions are still kept to neutralize charge. This reduced system containing 19 336 atoms is then used for the QM/MM calculations. An active region containing all residues within 8 Å from the (6−4)T−T residue was allowed to relax during the various QM/MM geometry optimizations carried out in this work.

The ChemShell QM/MM interface[57] was used for setting up and performing the QM/MM calculations. The DL_POLY[58] molecular dynamics module integrated in ChemShell was employed for evaluating the MM energy. The AMBER parameters were passed on to DL_POLY directly via the AMBER-interface available in

(43) Domratcheva, T.; Schlichting, I. *J. Am. Chem. Soc.* **2009**, *131*, 17793–9.
(44) Li, J.; Liu, Z.; Tan, C.; Guo, X.; Wang, L.; Sancar, A.; Zhong, D. *Nature* **2010**, *466*, 887–890.
(45) Friesner, R. A.; Guallar, V. *Annu. Rev. Phys. Chem.* **2005**, *56*, 389–427.
(46) Lin, H.; Truhlar, D. G. *Theor. Chem. Acc.* **2007**, *2*, 185–199.
(47) Senn, H. M.; Thiel, W. QM/MM Methods for Biological Systems. In *Atomistic Approaches in Modern Biology*; Reiher, M., Ed.; Springer: Berlin, 2007.
(48) Senn, H. M.; Thiel, W. *Angew. Chem., Int. Ed.* **2009**, *48*, 1198–1229.
(49) Davis, I. W.; Leaver-Fay, A.; Chen, V. B.; Block, J. N.; Kapral, G. J.; Wang, X.; Murray, L. W.; W. B. A. III; Snoeyink, J.; Richardson, J. S.; Richardson, D. C. *Nucleic Acids Res.* **2007**, *35*, 375–83.
(50) Jorgensen, W. L.; Chandrasekhar, J.; Madura, J. D.; Impey, R. W.; Klein, M. L. *J. Chem. Phys.* **1983**, *79*, 926–935.
(51) Duan, Y.; Wu, C.; Chowdhury, S.; Lee, M. C.; Xiong, G.; Zhang, W.; Yang, R.; Cieplak, P.; Luo, R.; Lee, T.; Caldwell, J.; Wang, J.; Kollman, P. *J. Comput. Chem.* **2003**, *24*, 1999–2012.
(52) Case, A. D.; et al. *AMBER 10*; University of California: San Francisco, 2008.
(53) Perez, A.; Marchan, I.; Svozil, D.; Sponer, J.; Cheatham, T. E., III; Laughton, C. A.; Orozco, M. *Biophys. J.* **2007**, *92*, 3817–3819.
(54) Bayly, C. I.; Cieplak, P.; Cornell, W. D.; Kollman, P. A. *J. Phys. Chem.* **1993**, *97*, 10269–10280.
(55) Shao, J.; Tanner, S. W.; Cheatham, T. E., III. *J. Chem. Theory Comput.* **2007**, *3*, 2312–34.
(56) Zhang, Y.; Kua, J.; McCammon, J. A. *J. Phys. Chem. B* **2003**, *107*, 4459–63.
(57) Sherwood, P.; et al. *J. Mol. Struct. (THEOCHEM)* **2003**, *1*, 632.
(58) Smith, W.; Yong, C.; Rodger, P. *Mol. Simul.* **2002**, *28*, 385.

ChemShell. The QM/MM geometry optimization tasks were performed via the DL-FIND optimizer (see ref 59 and references therein) implemented in ChemShell. The QM−MM electrostatic interaction was described by including all MM point charges in the one-electron part of the QM Hamiltonian. The QM−MM boundary regions were treated via a link atom approach and the charge-shift scheme.[60]

On the QM side, the TURBOMOLE programm suite[61] was used to evaluate the QM energy and gradient. Both closed- and open-shell (radical or biradical) states of the QM-region were treated with Density Functional Theory (DFT). The B-LYP functional[62] in combination with the dispersion correction suggested by Grimme was employed[63] for the first round of structure optimizations. The B3-LYP functional[64] was then used for the second and final round of geometry optimization. The barrier estimates obtained at both BLYP-D/AMBER and B3LYP-D/AMBER levels are compared in Table 1 in the Supporting Information. The results discussed further below are those of the B3LYP-D/AMBER calculations.

Of special importance for the repair mechanism is the role played by the photolyase enzyme, which implies that the QM-region must not solely include the (6−4)T−T photolesion, but also the often-discussed histidine residues, as well as those residues H-bonded to the photolesion. We anticipate that a mechanism of population transfer, from a locally excited state with significant oscillator strength to a charge transfer state, is responsible for the electron transfer to the lesion, similar to other systems containing flavin as the chromophore.[65,66] However, to avoid expensive quantum chemical calculations, we consider the case where the electron-transfer step is already completed. Two different QM-regions (A) and (B) are defined. The QM-region (A), as depicted in Figure 2, contains the (6−4) T−T photolesion, crystal water (Wat, residue number 697), Gln-299, Lys247, as well as the two His365 and His369 residues (residue numbering according to the crystal structure[41]). The QM-region (B) is defined as the augmentation of the QM-region (A) by the isoalloxazine part of the FAD moiety. The force field parameters used for the remaining parts of the FAD residue (i.e., adenine, the two phosphate groups, etc.) are taken from those of the $FADH^{\bullet}$. Three different "states" are considered in this study as follows:

(i) Prior to electron uptake from the flavin chromophore, the system is in its neutral state. Here, the FAD residue is fully included in the MM-region, and the $FADH^{-}$ parameters are used. The QM-subsystem, that is, QM-region (A), is in its singlet ground state (closed-shell). (ii) After the electron-transfer step, the FAD chromophore, having lost an electron, is in its $FADH^{\bullet}$ form and described by the corresponding $FADH^{\bullet}$ force field parameters. The QM-subsystem (still QM-region (A)), having gained an electron, is treated as an open-shell system. This state is denoted in the following as the radical state (referring to QM-region (A)). Actually, the "radical state" is a biradical if we were to include the $FADH^{\bullet}$ residue, or at least its flavin part, in the QM-region; electron back transfer (QM-subsystem → $FADH^{\bullet}$) is therefore a recombination of the two radicals. (iii) To estimate the barrier of the biradical recombination, it is necessary to treat both radicals at the QM-level. For this purpose, the QM-region (B) is introduced, and the corresponding biradical state is treated as an open-shell system.

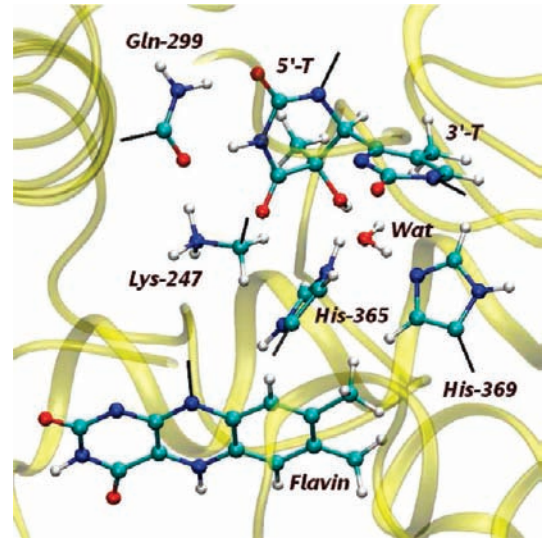

Figure 2. The QM-region (B) used to describe the biradical state of the photolesion in this QM/MM study. It contains the (6−4)T−T lesion, Gln-299, Lys242, His365, His369, isoalloxazine (Flavin) ring of the FADH chromophore, as well as the crystal water molecules denoted here as Wat. Black sticks are used to represent QM−MM bonds, which are capped by H-atoms. QM-region (A) is a subset of the QM-region (B) where the flavin part is excluded. Graphics prepared by the VMD package: http://www.ks.uiuc.edu/research/vmd/.

3. Results and Discussion

The protonation state of the two conserved Histidine residues, His365 and His369, as mentioned earlier, is one of the key factors influencing the repair mechanism of the (6−4)T−T photolesion. As part of the presented theoretical investigation, MD simulations with three different protonation states for these two residues have been performed. In the first simulation, neither of the histidine residues was protonated. Here, the deviations of the structures of the MD trajectory from the reference crystal structure are quite large. To visualize these deviations, the distance between the N_e and N_e' atoms (for the labeling, see Figure 3a) is plotted against simulation time and depicted in Figure 3b. As is evident from this figure, for the case where none of the histidines is protonated, there is a strong repulsion between these residues, leading to distances much larger than the experimentally observed one of 2.75 Å in the reference crystal structure. Thus, this particular protonation state can safely be ruled out. In the next MD simulation, only the His365 residue was protonated (at N_e), and the corresponding N_e-N_e' distance is again monitored in Figure 3b. Here, a much closer agreement with the experimental value is observed with fluctuations of 0.12 Å around 3.0 Å. Finally, the case where the His369 residue is protonated (at N_e') is studied. Again, the measured N_e-N_e' distances are quite close to the distance observed in the crystal reference structure; the deviations, however, are somewhat larger (0.18 Å) as compared to the His365 protonated case. The MD simulation hence shows that one of the two histidine residues indeed is protonated before the $FADH^{-}$ → (6−4)T−T electron transfer occurs, but there seems to be no clear preference. (In fact, our QM/MM calculations show that the barrier for the proton-exchange between the His365 and His369 residues is very low, but no productive pathway starting from the His369 protonated structure could be found (data not shown).) The protonation state of these two residues, on the other hand, is directly related to the pH-dependency of the repair activity of the (6−4) photolyase, as suggested by Schleicher et al.[37] In other

(59) Kästner, J.; Carr, J. M.; Keal, T. W.; Thiel, W.; Wander, A.; Sherwood, P. *J. Phys. Chem. A* **2009**, *113*, 11856–65.
(60) de Vries, A. H.; Sherwood, P.; Collins, S. J.; Rigby, A. M.; Rigutto, M.; Kramer, G. J. *J. Phys. Chem. B* **1999**, *103*, 6133–6141.
(61) Ahlrichs, R.; Bär, M.; Häser, M.; Horn, H.; Kölmel, C. *Chem. Phys. Lett.* **1989**, *162*, 165–169.
(62) Becke, A. D. *Phys. Rev. A* **1988**, *38*, 3098.
(63) Grimme, S. *J. Comput. Chem.* **2006**, *27*, 1787–1789.
(64) Becke, A. D. *J. Chem. Phys.* **1993**, *98*, 5648.
(65) Sadeghian, K.; Schutz, M. *J. Am. Chem. Soc.* **2007**, *129*, 4068–4074.
(66) Sadeghian, K.; Bocola, M.; Schutz, M. *J. Am. Chem. Soc.* **2008**, *130*, 12501–13.

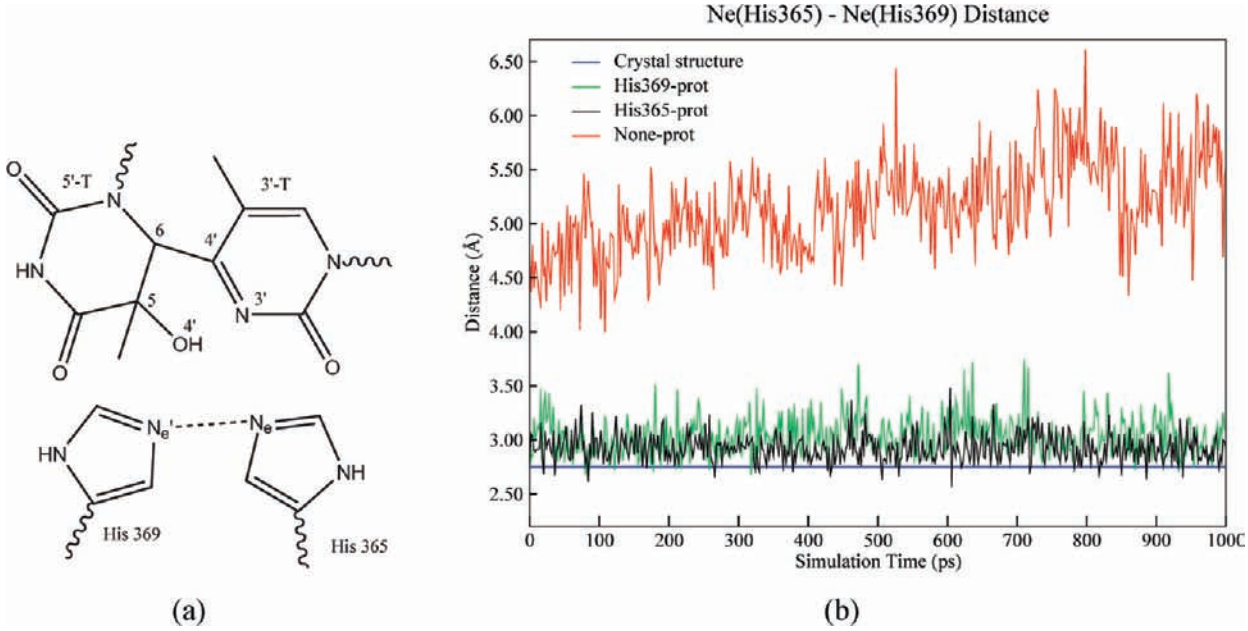

Figure 3. (a) Structure of the (6−4)T−T and the two Histidine residues where the N_e-N_e' distance is indicated. (b) The distance between the two nitrogen atoms of the His365 and His369 residues, N_e and N_e', respectively, is plotted against the simulation time. In the crystal structure,[41] a distance of 2.75 Å, indicated by the blue line, is observed.

words, the efficiency of the repair may well depend on whether one or the other histidine is protonated as the electron transfer from $FADH^-$ occurs.

As is evident from the crystal structure, the N3′ and O4′ atoms of the 3′-T base belong to the sites that are in close contact with both Histidines. To have a crude estimate on the likelihood of protonation of these two sites by one of the histidine residues, the distances between the corresponding nitrogen atom (N_e for His365 protonated and N_e' for the His369 protonated) and the N3′ or O4′ atoms of the 3′-base have been analyzed (see Figure SI-1 in the Supporting Information). In the His-365 protonated case, the N_e-O4' and N_e-N3' distances fluctuate by 0.15 and 0.32 Å around 3.0 and 3.8 Å, respectively. In the His-369 protonated case, on the other hand, the $N_e'-O4'$ and $N_e'-N3'$ fluctuate by 0.21 and 0.27 Å about larger values, that is, 4.0 and 5.0 Å, respectively. On the basis of these results, one may therefore conclude that the His-365 protonated residue has a higher chance of protonating the (6−4)T−T photoproduct after photoexcitation.

The starting structure for the QM/MM calculation has been prepared using the procedure described in section 2. The active site was then optimized at the B3LYP-D/AMBER level, and the resulting minimized structure, denoted as (**I**), is shown schematically in Figure 4. Here, the His365 residue remains protonated after QM/MM geometry minimization and forms a hydrogen bond with the O4′ atom of (6−4)T−T (see Figure 4 for the definition of the atom labels used throughout in this work). In addition, a hydrogen-bonding network involving the hydroxy group at O4′, the crystal water molecule (Wat), and the nitrogen atom (N_e') of the His369 residue is observed. The (**I**) structure was then used as a starting geometry for the optimization of the radical state by employing the QM/MM settings (open-shell doublet state for the QM-region (A) + $FADH^\bullet$ parameters for the FAD chromophore) as already described in section 2. The resulting minimized structure, denoted as $(\mathbf{I})^\bullet$, is very similar to the (**I**) structure.

Starting from the His365 protonated $(\mathbf{I})^\bullet$ structure, three different reaction pathways were studied: (i) OH-transfer as proposed by Domratcheva et al.,[43] (ii) initial water formation as suggested by Maul et al.,[41] and (iii) initial protonation of the N3′ atom via the protonated His365.

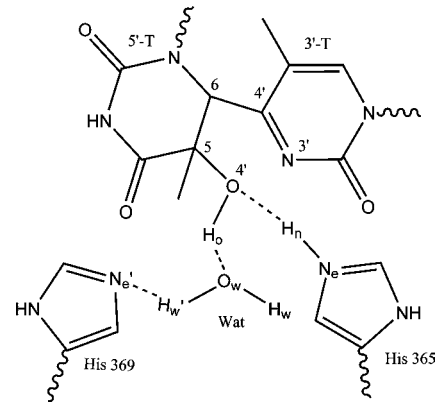

Figure 4. Schematic representation of the QM/MM-optimized (**I**) structure. The His369 residue is protonated and acts as a donor in a H-bond with the O4′ atom of the 3′-T base. Another hydrogen-bonding network involving the hydroxy group of the 3′-base, the water molecule (Wat), and the His-369 residue is also shown. The QM/MM-optimized structure of its radical counterpart, the $(\mathbf{I})^\bullet$ structure, is similar to this structure and therefore not depicted here.

All three pathways have been studied by following relaxed energy paths (REP), along the corresponding reaction coordinates.

i. Repair via OH-Transfer. Here, starting from the $(\mathbf{I})^\bullet$ structure, a reaction coordinate, Q_{OH}, was chosen to form the C4′−O4′ bond and to break the C4′−C6′ bond. Such a reaction coordinate can be defined as a linear combination of the C4−O4′ and C6−C4′ bond distances ($Q_{OH} = r(C4-O4') - r(C6-C4')$). The energy profile along this REP is shown in Figure SI-2 (see the Supporting Information). The OH-transfer process within the (6−4)T−T binding pocket of the (6−4) photolyase is energetically not feasible. An energy difference of more than 50 kcal/mol is observed between the initial $(\mathbf{I})^\bullet$ and the final (6−4)-$OH^\bullet$ structure obtained at the end of this REP (Q_{OH} =

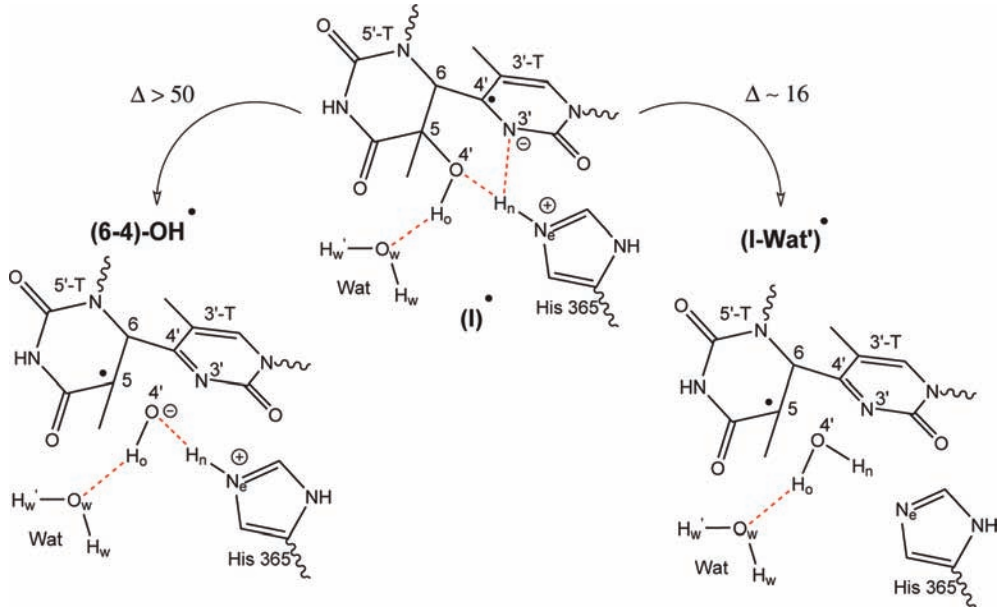

Figure 5. The initial (**I**)• and the (6−4)-OH• structure picked out at the end of the OH-transfer path. The (I−Wat′)• structure, corresponding to the minimum geometry obtained after overcoming the barrier along the water formation path, is also shown. The corresponding QM/MM paths are shown in Figure SI-2. The barrier estimates (Δ in kcal/mol) are also indicated.

−1.0 bohr depicted in Figure SI-2). Furthermore, no stable minimum structure could be reached along this reaction pathway.

ii. Repair via Water Formation. Detachment of a hydroxy group from the 5′-T base and deprotonation of the His365 residue leads to the formation of a (second) water molecule, denoted as Wat′, in the (6−4)T−T binding pocket. This process can be investigated by employing a linear combination of the H_n−O4′ and C5−O4′ bond distances ($Q_W = r(H_n\text{−}O4') - r(C5\text{−}O4')$) as a reaction coordinate. The energy profile along this REP is also shown Figure SI-2. The highest energy point along the REP is roughly 16 kcal/mol above that of the (**I**)• structure. The minimum structure corresponding to the case where the Wat′ is formed, denoted as (I−Wat′)• and shown in Figure 5, however, is 4 kcal/mol above the (**I**)• structure. The orientation of the two water molecules, Wat and Wat′, is similar to that of the water dimer.

Even though the (I−Wat′)• structure is less stable than the (**I**)• structure, further possible pathways starting from the former were studied. For example, the possibility that one of the two histidine residues, both being deprotonated at the (I−Wat′)• stage, can be protonated by one of the two water molecules (Wat or Wat′) was explored. Such attempts, however, failed. Only a high energy barrier (more than 35 kcal/mol) and no stable structure along the corresponding REPs could be found.

Finally, we decided to investigate the stability of the [(I−Wat′)•−FADH•] species by performing a QM/MM geometry optimization within QM-region (B). Here, the [(I−Wat′)•−FADH•] biradical structure was found to be very unstable, and a restraint-free QM/MM geometry minimization starting from such a conformation directly leads to the initial (**I**) structure without any barrier in between.

Overall, the water formation as a first step after electron transfer is certainly more probable than the direct OH transfer as is evident from Figure 5, yet the (I−Wat′)• radical complex does not lead to the repaired form.

iii. Repair via N3′ Protonation. Another possibility considered in this study is the protonation of the N3′ position of the 3′-base via the neighboring protonated His365 residue in the (**I**)• structure. This is the initial step of the repair mechanism presented in this study, which is shown schematically in Figure 6. Protonation of the N3′ position by the His365 residue is motivated by the $\alpha-\beta$ spin density difference plot for the QM-region of the (**I**)• structure depicted in Figure 7. The distribution of the radical, being mainly on the 3′-T base, shows that the N3′ position of the latter residue is much more amenable for protonation than the O4′ atom of the 5′-T base discussed previously. It should be mentioned that in the crystal structure and all MD snapshots obtained in this study, the O4′ atom is pointing away from the N3′ position. This means that the intramolecular protonation of the N3′ from O4′ is geometrically hindered.

Starting from the (**I**)• structure and using the QM-region (A), the REP along the proton transfer coordinate Q_1, where $Q_1 = r(N3'\text{−}H_n) - r(N_e\text{−}H_n)$, leads to the stable (**II**$_a$)• structure, also depicted in Figure 6. The latter is about 16 kcal/mol below the (**I**)• structure, and almost no barrier is observed for this protonation step (see Figure SI-3).

Having reached the (**II**$_a$)• structure, one has to consider a competing and destructive pathway, the [(**II**$_a$)•−FADH•] charge recombination, which eventually leads to the initial (**I**) structure already shown in Figure 4. To investigate this process, a QM/MM-REP along a coordinate that involves the H_n transfer from the N3′ atom of the 3′-T base to the N_e of the His365 residue ($Q^n_{rec} = r(N3'\text{−}H_n) - r(N_e\text{−}H_n)$) has been studied using the QM-region (B). For this biradical recombination step, an energy barrier of only 2 kcal/mol is estimated (see Figure SI-4). The efficiency of this process could be due to the H-bond network N3′−H_n−N_e between the (6−4)T−T photoproduct and the His365 residue, which is present in the (**II**$_a$)• conformation (cf., Figure 6).

The repair process can be continued by disruption of the above-mentioned H-bond network, that is, by following a REP along the N3′−N_e distance (reaction coordinate Q_{2a}) in the direction where the photolesion and the His365 residue are separated. The structure obtained after overcoming an energy

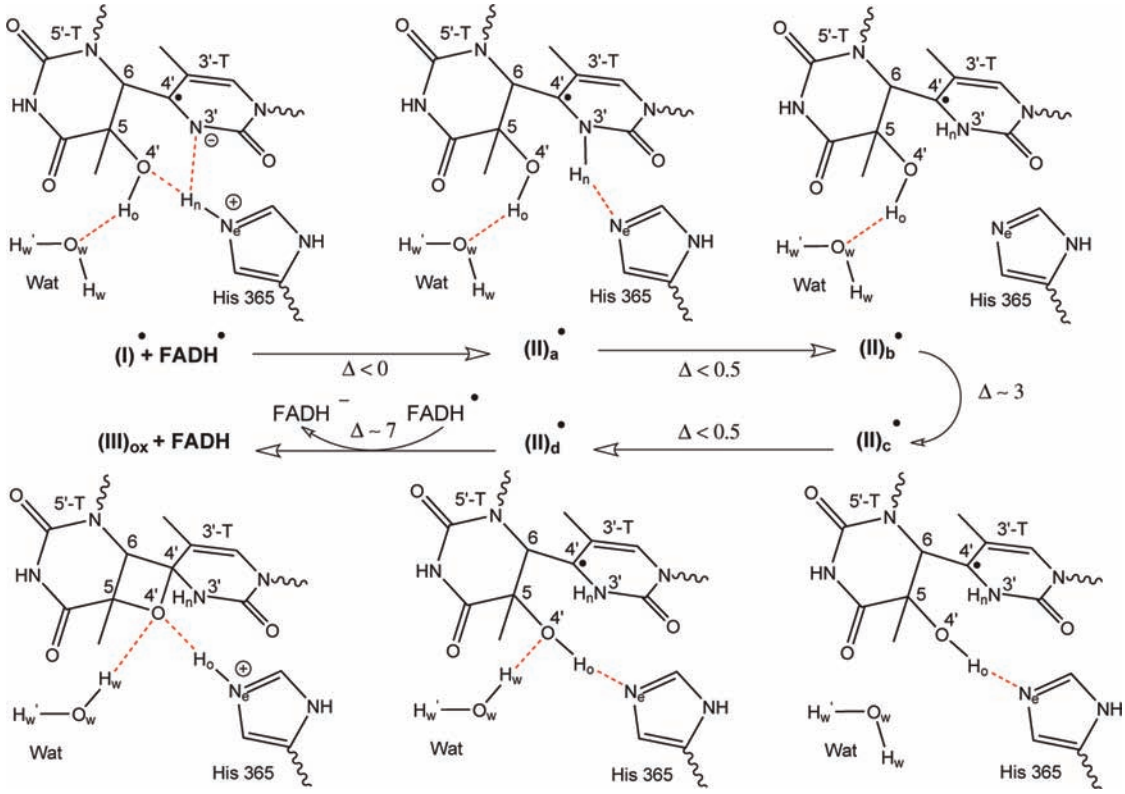

Figure 6. Series of structures involved in the repair mechanism after the absorption of the first photon. In addition, the barrier estimates (Δ in kcal/mol) for the transitions $\mathbf{I}^{\bullet} \rightarrow \mathbf{II}^{\bullet} \rightarrow (\mathbf{III})_{ox}$ are also indicated.

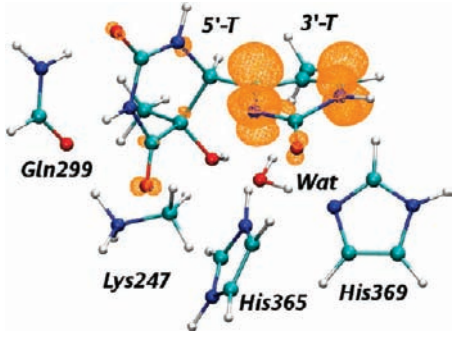

Figure 7. $\alpha-\beta$ spin density difference plot for the QM-region of the $(\mathbf{I})^{\bullet}$ structure. The radical is mainly distributed in the 3′-T base where the N3′ atom is the most likely position to accept a proton from the His365 residue.

difference of less than 0.5 kcal/mol (cf., Figure SI-3) is denoted as $(\mathbf{II}_b)^{\bullet}$ and depicted in Figure 6. The $(\mathbf{II}_b)^{\bullet}$ structure lies energetically approximately 1 kcal/mol below the previous $(\mathbf{II}_a)^{\bullet}$ structure. The barrier for the competing $[(\mathbf{II}_b)^{\bullet}-\mathrm{FADH}^{\bullet}]$ recombination is now estimated as about 3 kcal/mol (see Figure SI-4). As expected, the separation of the 3′-base and His365 residue has increased the barrier of the biradical recombination step, which would otherwise be destructive for the repair process.

In the $(\mathbf{II}_b)^{\bullet}$ structure, the hydroxy group at the 5′-base is involved in a hydrogen-bonding interaction with the Wat molecule. This H-bond can be disrupted by inducing another H-bond, between the hydroxy group and the N_e atom of the His365, which has been deprotonated. A QM/MM REP along the corresponding coordinate, $Q_{2b} = r(O_w-H_o) - r(N_e-H_o)$, was explored as shown in Figure SI-3. The structure obtained after the formation of the new H-bond, denoted as $(\mathbf{II}_c)^{\bullet}$ and depicted in Figure 6, is about 1.5 kcal/mol above the $(\mathbf{II}_b)^{\bullet}$ structure, and a barrier of about 3 kcal/mol has to be surmounted.

From the $(\mathbf{II}_c)^{\bullet}$ structure, there is a steep and almost barrierless path leading toward the $(\mathbf{II}_d)^{\bullet}$ structure depicted in Figure 6, which is roughly 22 kcal/mol lower in energy than the initial $(\mathbf{I})^{\bullet}$ structure (cf., Figure SI-3). This path can be decomposed into two relaxation parts along two different reaction coordinates. The first part is dominated by a 90° rotation of the OH group (of the 5′-T base) away from the 3′-T base where the H-bonding interaction with the His365-N_e is retained. The corresponding QM/MM REP is shown in Figure SI-3, where the dihedral angle $Q_{2c} = \tau(C6-C5-O4'-H_o)$ is used as a reaction coordinate. The structure so obtained is schematically rather similar to the $(\mathbf{II}_c)^{\bullet}$ structure and therefore not depicted in Figure 6 (see Figure SI-5 for a comparison of hese two structures). The second relaxation part involves the formation of a H-bond between the H_w atom of the Wat molecule and the O4′ atom of the 5′-base, hence leading to the $(\mathbf{II}_d)^{\bullet}$ structure.

One may continue following the repair process by taking the $(\mathbf{II}_d)^{\bullet}$ structure and considering a REP along the coordinate responsible for the O4′-transfer from the C5 position of the 5′-base to the C4′ position of the 3′-base, Q_3 defined as $r(O4'-C4') - r(O4'-C5)$. From the energy profile along Q_3, a barrier of about 50 kcal/mol can be estimated (see Figure SI-6) where the structure obtained after overcoming this high barrier resembles the oxetane intermediate, which has been discussed extensively in the literature in connection with the (6−4)T−T repair. This geometry is denoted here as oxetane-$(\mathbf{III}^{\bullet})$ (or $(\mathbf{III})^{\bullet}_{ox}$ for short) to indicate the fact that we are still dealing with the radical state with respect to the QM-region (A).

Formation of the $(\mathbf{III})^{\bullet}_{ox}$ radical competes with the biradical recombination step, which, in contrast to the former, requires

the explicit H_o proton transfer back to the His365 residue. For the corresponding QM/MM calculations, the reaction coordinate Q^o_{rec}, where $Q^o_{rec} = r(O4'-H_o) - r(N_e-H_o)$, and QM-region (B) are used. The $[(\mathbf{II}_d)^\bullet-FADH^\bullet]$ recombination along the Q^o_{rec} coordinate involves a barrier of only 7 kcal/mol (cf., Figure SI-4) and leads to the formation of the $(\mathbf{III})_{ox}$ oxetane depicted in Figure 6.

Evidently, formation of the neutral $(\mathbf{III})_{ox}$ structure is energetically much more probable than the formation of the $(\mathbf{III})^\bullet_{ox}$ oxetane radical counterpart (50 vs 7 kcal/mol). A key issue here is the lifetime of the $FADH^\bullet$ radical. During the revision of this Article, Li et al.[44] reported the results of their ultrafast spectroscopy measurements, where they show that the lifetime of the $FADH^\bullet$ radical is in the order of some tens of nanoseconds. This is in a good agreement with the barrier we have obtained for the $[(\mathbf{II}_d)^\bullet-FADH^\bullet]$ biradical recombination step. Direct formation of $(\mathbf{III})^\bullet_{ox}$ from the $(\mathbf{II}_d)^\bullet$ structure can therefore be safely precluded.

One possible outcome of this finding is that the repair process continues on the ground state (i.e., thermally). To investigate this possibility, the thermal splitting of the oxetane into the repaired form, denoted here as the **TpT**-form, is also studied. For the corresponding QM/MM calculations, the QM-region (A) treated as a closed-shell system and the force field parameter of $FADH^-$ are employed. The QM/MM REP obtained along the reaction coordinate Q_4 ($Q_4 = r(C4'-O4') + r(C5-C6) - r(C4'-C6) - r(C5-O4')$) is shown in Figure SI-7, where a barrier of about 53 kcal/mol is to be surmounted before reaching the repaired **TpT** structure. The latter is 9 kcal/mol below the initial damaged (**I**) structure. It is interesting to note that the photolyase enzyme, especially the His365 residue, does not influence this barrier, for example, via protonation. To illustrate this point, we have considered a two-dimensional relaxed energy surface along two coordinates: Q_4 and Q_8 with $Q_8 = r(N_e-H_o) - r(O4'-H_o)$. On the basis of QM/MM calculations carried out using both reaction coordinates as restraints, an interpolated surface is obtained and depicted in Figure SI-7. It clearly shows that the His365 residue does not play any catalytic role in the thermal splitting of the oxetane intermediate.

It is well-known that the oxetane structure is energetically less stable than the initial (6−4) form (see refs 33, 43 and references therein). Starting from the $(\mathbf{III})_{ox}$ structure, a possible destructive pathway toward the initial damaged (**I**) structure would be the reprotonation of the O4′-atom through the His365 residue as well as C4−O4′ bond cleavage (see Figure 8). The QM/MM REP along the corresponding coordinate, Q_6 ($Q_6 = r(N3'-H_o) - r(O4'-H_o)$), is also shown in Figure SI-7, where, after overcoming a barrier of about 16 kcal/mol, a conformation similar to $(\mathbf{II}_b)^\bullet$ is reached (cf., Figure 8). The resulting minimized structure is denoted as ($\mathbf{II}_b$) and lies 19 kcal/mol above the initial damaged (**I**) structure. The latter can be reached through a proton back transfer from the N3′-atom of the 3′-T base to the N_e-atom of the His365 residue. The estimated barrier along the corresponding coordinate, Q_7 ($Q_7 = r(N3'-H_o) - r(N_e-H_o)$), is about 2 kcal/mol (see Figure SI-7).

These results show that the formation of the (metastable) oxetane intermediate is the main outcome of the initial photoexcitation. The thermal repair of the oxetane on the ground-state surface is energetically very demanding and cannot compete with the destructive processes, which only lead to the initial (6−4)T−T form of the photolesion. This would mean that a repair process utilizing a single photon is extremely inefficient, if not impossible. In fact, Li et al.[44] have shown

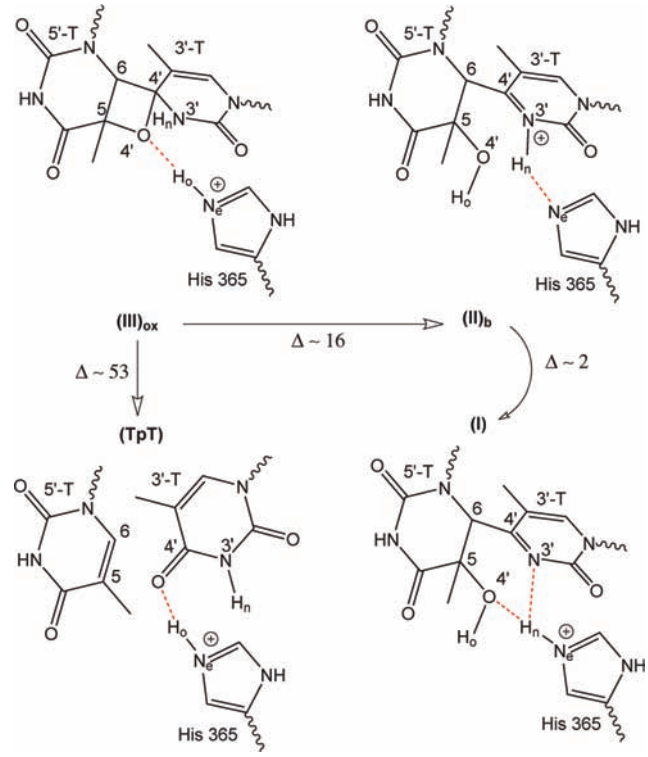

Figure 8. Series of structures involved in the thermally driven transitions after reaching the neutral $(\mathbf{III})_{ox}$ oxetane together with the corresponding barrier estimates (Δ in kcal/mol).

that the absorption band of the repaired thymine monomers appears after some hours and under continuous white light conditions. As mentioned in the Introduction, there are several experimental findings that support the idea that the oxetane species can be easily split into the repaired form via photoexcitaion and/or electron transfer. We therefore propose that a second photoexcitation of $FADH^-$ is required to complete the repair process.

Absorption of a second photon by the FAD chromophore, being again in its reduced anionic $FADH^-$ form at the $(\mathbf{III})_{ox}$ stage, is followed by the subsequent second electron transfer from the former to the $(\mathbf{III})_{ox}$ oxetane. This second photoinduced electron-transfer step can promote the system directly into the energetically higher $(\mathbf{III})^\bullet_{ox}$ structure (+18 kcal/mol relative to the $(\mathbf{I})^\bullet$; see Figure SI-6), which has been mentioned previously. (Indeed, the $(\mathbf{III})^\bullet_{ox}$ structure can also be obtained by taking the $(\mathbf{III})_{ox}$ geometry, choosing the QM-region (A), and performing QM/MM geometry optimization where the QM subsystem is treated as a radical.) The reaction coordinate Q_4 used for the thermal splitting of the neutral oxetane $(\mathbf{III})_{ox}$ can also be used for the splitting of the $(\mathbf{III})^\bullet_{ox}$ radical. The resulting QM/MM REP, depicted in Figure SI-6, shows that the C5′−O4′ bond cleaves almost barrierless ($\Delta < 0.5$ kcal/mol), leading to the $(\mathbf{IV})^\bullet$ structure (see Figure 9). The sudden drop in the QM/MM energy is due to the protonation of the O4′ atom by the His365 residue during the C5−O4′ bond cleavage (corresponding mainly to a coordinate orthogonal to Q_4). The resulting protonated and stable $(\mathbf{IV})^\bullet$ structure is now 23 kcal/mol below the $(\mathbf{III})^\bullet_{ox}$ structure.

The next step in the repair process is the cleavage of the C4′−C6 bond. For this purpose, a QM/MM REP, starting from the $(\mathbf{IV})^\bullet$ structure, along the $r(C4'-C6)$ bond distance, Q_5, has been investigated. As shown in Figure SI-6, a barrier of 9 kcal/

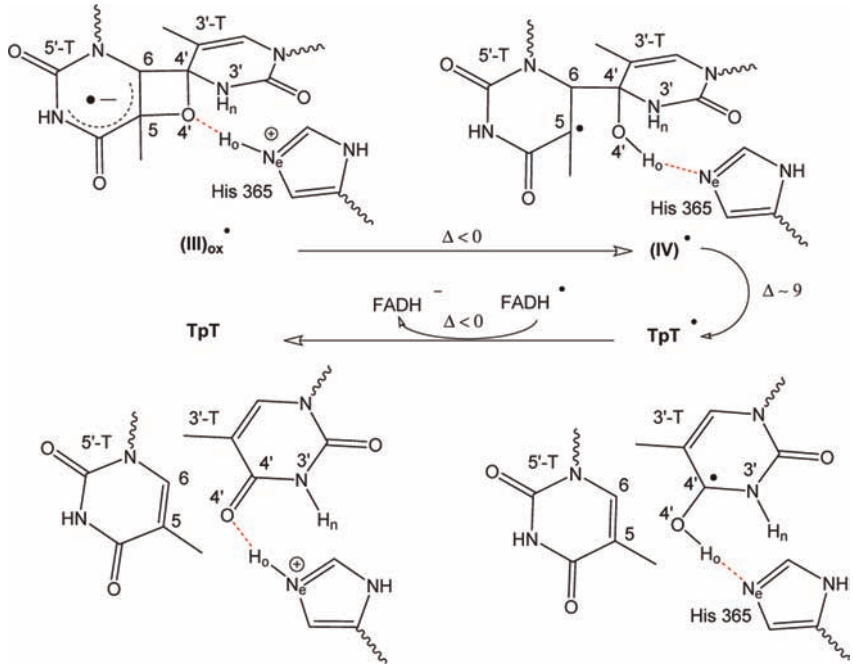

Figure 9. Series of structures involved in the repair mechanism after the absorption of the second photon. In addition, the barrier estimates (Δ in kcal/mol) for the transitions $(\mathbf{III})_{ox} \rightarrow (\mathbf{IV})^{\bullet} \rightarrow (\mathbf{TpT})^{\bullet}$ are also indicated.

mol is required for this step, leading to the $(\mathbf{TpT})^{\bullet}$ structure, which is 17 kcal/mol below the initial $(\mathbf{I})^{\bullet}$ structure and depicted in Figure 9. The latter process has to compete with the $[(\mathbf{IV})^{\bullet}-\mathrm{FADH}^{\bullet}]$ recombination step along the Q^{o}_{rec} coordinate, leading to back the $(\mathbf{III})_{ox}$ conformation. Here, a barrier of about 7 kcal/mol is estimated (see Figure SI-8).

The final step in the repair process is the electron back transfer to $\mathrm{FADH}^{\bullet}$, as well as deprotonation of the oxygen O4′, now at the C4 position of the 3′-base. This last step has been studied via the $[(\mathbf{TpT})^{\bullet}-\mathrm{FADH}^{\bullet}]$ recombination along the Q^{o}_{rec} coordinate where the QM-region (B) was employed for the QM/MM calculations. A barrierless path is observed (Figure SI-8), which leads to the fully repaired thymine monomers (**TpT**-form) depicted in Figure 9. It is noteworthy that, in contrast to the case of the thermal splitting of $(\mathbf{III})_{ox}$ oxetane, the conserved His365 is the key residue that assists the splitting of the $(\mathbf{III})^{\bullet}_{ox}$ oxetane radical via protonation (in both back and forth directions). This is in line with the previous studies, which show that the mutation of this very residue leads to inactivation of the enzyme.[41,22]

4. Summary and Conclusion

As is evident from the crystal structures of the (6−4) photolyase bound to (6−4)T−T and repaired ds-DNA, the overall effect of the (6−4) photorepair is to transfer an oxygen and a hydrogen atom/proton from the 5′-base to the 3′-base. This transfer is initiated by the photoexcitation and subsequent electron transfer from the FAD chromophore found in the (6−4) photolyase. With the main goal of comparing the energetic feasibility of some of the pathways that connect the (6−4) photolesion to its repaired form, a series of QM/MM calculations have been performed.

The QM/MM calculations presented here show that the simultaneous transfer of the oxygen and hydrogen atoms, in form of a hydroxyl group, as suggested by the gas-phase calculations of Domratcheva and Schlichting,[43] is not feasible in the enzyme. The formation of a (second) water molecule in the photolesion binding pocket, as proposed by the Maul et al.,[41] seems also not to be a productive step regarding the overall repair process.

On the basis of the QM/MM results obtained and presented in section 3, a different mechanism is proposed and schematically displayed in Figure 10. The QM/MM energies of the (**I**) and $(\mathbf{I})^{\bullet}$ structures are taken as reference for the processes occurring either before or after the electron uptake from FADH^{-}. These processes are depicted in the lower and upper half of this figure, respectively. In the presented mechanism, we have observed numerous photolesion ↔ photolyase proton transfer processes. The complete transfer of the oxygen atom requires two photons and is shown to occur via (i) photoinduced formation of the oxetane intermediate, followed by (ii) the photoinduced splitting of the latter. To aid the discussion, it is convenient to describe the whole repair mechanism along the two "H^{+} transfer" and "repair" (O-transfer) coordinates. On the basis of the data obtained in this study, a schematic view of the energy surfaces, for both neutral and radical states, projected on these two coordinates is displayed in Figure 11.

The first part of the reaction cascade, being initiated by the first photoexcitation, starts from the $(\mathbf{I})^{\bullet}$ structure and leads to the $(\mathbf{III})_{ox}$ structure, via proton exchange between the photolesion and the enzyme (through His365). The intermediate $(\mathbf{II})^{\bullet}$ structures are all energetically accessible. The rather low efficiency of the enzyme can be traced back to those destructive radical recombination processes, which lead to the initial (6−4)T−T form (shown by red arrows in Figure 10). The $(\mathbf{II}_{d})^{\bullet}$ structure can undergo charge recombination, hence forming the neutral $(\mathbf{III})_{ox}$ intermediate via reprotonation of the His365 residue. For this step, a barrier of 7 kcal/mol is obtained, which is in good agreement with the lifetime of some tens of nanoseconds measured for the $\mathrm{FADH}^{\bullet}$ radical.[44]

The neutral $(\mathbf{III})_{ox}$ oxetane structure is then again photoexcited by the second photon. Upon electron transfer from the excited

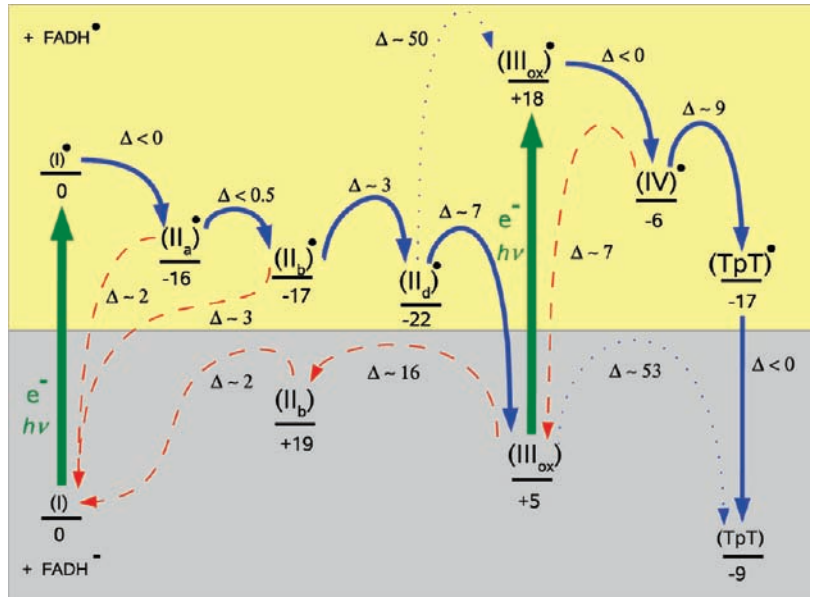

Figure 10. A schematic representation of the proposed mechanism. Structures indicated on the top half correspond to the radical state with respect to QM-region (A), whereas those on the bottom represent closed-shell structures. Solid thick green lines indicate absorption of a photon followed by the electron transfer from the excited $FADH^{-}$* to the photolesion. Solid blue lines represent processes that drive the system toward repair. The red dashed lines, on the other hand, are used to indicate processes that are destructive with respect to the overall efficiency of the repair process. The pathway involving the direct formation of the radical oxetane species without the absorption of a second photon is shown by the dotted line. Note that the upper → lower transitions (yellow → gray) represent biradical recombination processes where the QM-region (B) has been employed for corresponding QM/MM calculations. The QM/MM energies and barrier estimates are in kcal/mol.

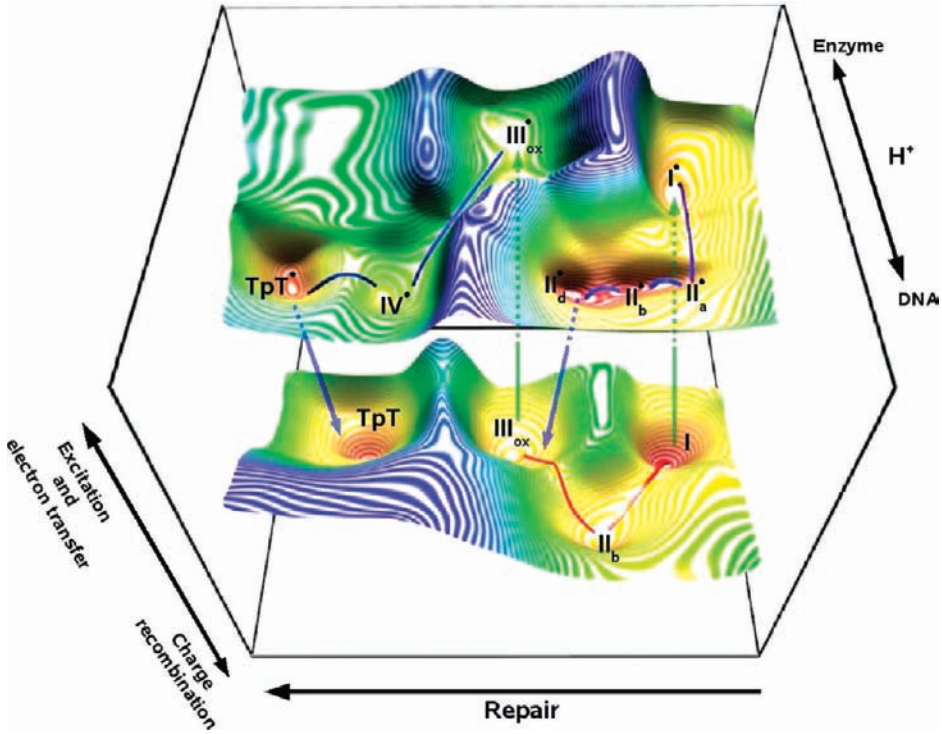

Figure 11. A schematic view of the two-dimensional relaxed energy surface along the two "H^+ transfer" and "repair" coordinates adapted from the QM/MM calculations presented in this study. The green arrows indicate photoexcitations promoting the system to the radical state. The path highlighted by the blue lines indicates the path taken along the repair cascade. The path indicated by the red lines represents the destructive thermal processes connecting the $(\mathbf{III})_{ox}$ oxetane to the initial (6−4)T−T form of the photolesion.

$FADH^{-}$ chromophore, the system is promoted to the radical $(\mathbf{III})^{\bullet}_{ox}$ conformation. The splitting of the latter leading to the $(\mathbf{IV})^{\bullet}$ structure is again mediated by the photolyase, via protonation from the His365 residue. The last step on the radical state is the cleavage of the C4−C6 bond, hence forming the $(\mathbf{TpT})^{\bullet}$ species. The final step in the repair process is the transfer of the proton back to the His365 residue as well as charge recombination, both resulting in the repaired **TpT** form.

Overall, it has been shown that the repair is not straightforward and two photons are required to complete the repair process. The latter condition, together with some of the charge recombination steps presented in this study, account for the

rather low repair efficiency of the (6−4) photolyase enzyme. The His365 residue, found in the photolesion binding pocket of the enzyme, is found to be the key residue for the catalytic proton exchange processes taking place as part of the proposed repair cascade, in agreement with previous experimental findings.

Acknowledgment. We thank Dr. Paul Sherwood for providing the CHEMSHELL QM/MM interface. Financial support from the Deutsche Forschungsgemeinschaft (DFG), project number SCHU 1456/7-1, is gratefully acknowledged.

Supporting Information Available: Complete refs 52 and 57 and additional figures and tables. This material is available free of charge via the Internet at http://pubs.acs.org.

JA108336T